Intracellular pH Sensing

DOI: 10.1002/anie.201203866

Localized Intracellular pH Measurement Using a Ratiometric Photoinduced Electron-Transfer-Based Nanosensor**

María J. Marín, Francisco Galindo, Paul Thomas, and David A. Russell**

Dedicated to Professor Miguel A. Miranda on the occasion of his 60th birthday

Hydrogen ions are an important intracellular species. In eukaryotic cells the function of several organelles is dependent on the pH in each of those individual organelles.[1] The pH in the cytosol and the nucleus is typically 7.2–7.4, the secretory and the endocytic pathways have a lower pH, while the acidic organelles, such as endosomes and lysosomes, typically have a pH as low as 4.0–5.5.[1a,b] Disruption of the pH within the different organelles may lead to dysfunction of the affected organelle and ultimately to a diseased state. For example, tumor cells have been shown to have an abnormal cellular pH[2] and disturbances in the pH of the acidic organelles have been associated with renal failure,[3] oncological processes,[4] and with the so called lysosomal storage disorders.[5] With consideration of the large number of diseases related to abnormal values of pH in the acidic organelles it is important to develop new tools, to supplement those molecular probes that already exist,[6] to quantify the hydrogen ion concentration.

Ratiometric fluorescence-based nanosensors are an example of a robust tool for the sensing and quantification of ions of biological interest.[7] Kopelman and co-workers designed PEBBLEs (probes encapsulated by biologically localized embedding), ratiometric fluorescence nanosensors, for the intracellular measurement of pH.[8] Since then, a number of ratiometric fluorescence nanosensors for pH have been reported based on polymeric nanoparticles,[9] silica nanoparticles,[10] quantum dots,[11] cellulose nanocrystals,[12] latex nanobeads,[13] and zeolite-based nanoparticles.[14] There have been some reports on the internalization of ratiometric fluorescence pH nanosensors by cells,[15] with localization of the nanoprobes in the cytoplasm[16] or within acidic organelles.[17] Other studies have reported measurements of a change in intracellular pH values using dual ratiometric fluorescence nanoprobes.[18] Recently, a ratiometric polymeric nanoprobe composed of three fluorophores has been reported for intracellular pH measurements.[19]

Fluorescent photoinduced electron-transfer (PET) based pH molecular probes have been widely studied.[20] Previously, we have reported an anthracene-based PET pH probe with a readily tunable pK_a that accumulated in acidic organelles within Raw 264.7 macrophage cells.[21] The self-assembly of such PET-based pH probes onto gold nanoparticles has not been previously described.

Herein, we report a fluorescence pH nanosensor that provides, for the first time, precise localized determination of pH from within acidic organelles. The ratiometric nanosensor consists of a thiolated anthracene molecule as a fluorescent PET-based pH ligand (**1**) and a thiolated rhodamine ligand (**2**), both self-assembled onto the surface of a gold nanoparticle (**3**, Figure 1). The synthesized fluorescence-based pH

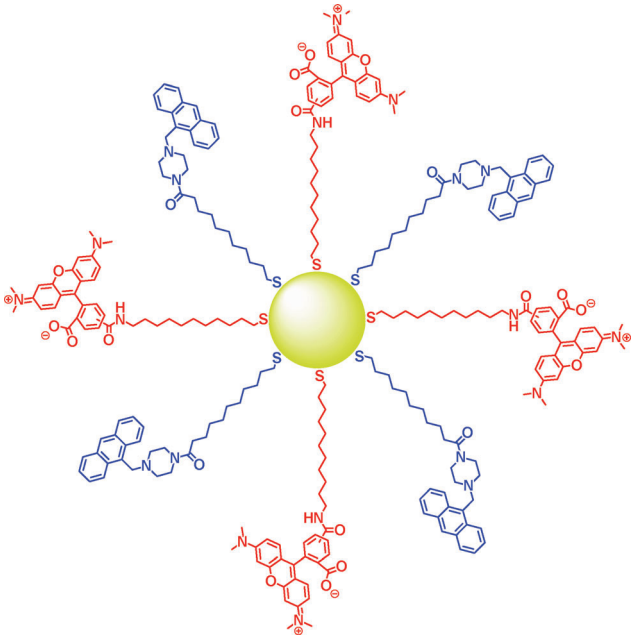

Figure 1. The pH nanosensor **3**: gold nanoparticle stabilized with the anthracene (**1**, blue) and rhodamine (**2**, red) derivatives.

[*] M. J. Marín, Prof. D. A. Russell
School of Chemistry, University of East Anglia
Norwich, Norfolk NR4 7TJ (UK)
E-mail: d.russell@uea.ac.uk
Dr. F. Galindo
Departamento de Química Inorgánica y Orgánica
Universitat Jaume I, 12071 Castellón de la Plana (Spain)
E-mail: francisco.galindo@uji.es
Dr. P. Thomas
School of Biological Sciences, University of East Anglia
Norwich, Norfolk NR4 7TJ (UK)

[**] The authors acknowledge the School of Chemistry, University of East Anglia, for a studentship for M.J.M. F.G. acknowledges the financial support of the Spanish MICINN (project number CTQ2009-09953). The authors are grateful to Prof. Tom Wileman (Norwich Medical School, UEA) for the CHO cells used, to Dr. Colin McDonald (School of Chemistry) for assistance with the TEM images and to John Wood (School of Pharmacy) for assistance with the error calculation.

Supporting information for this article including experimental details is available on the WWW under http://dx.doi.org/10.1002/anie.201203866.

nanosensor was endocytosed by Chinese Hamster Ovary (CHO) cells and the ratiometric fluorescence intensity of the nanosensor **3** was used to determine the intracellular pH of specific regions within the cells by combined confocal fluorescence microscopy and spectroscopy. The endocytosis of the pH nanosensor was confirmed by measuring the emission spectrum of the two fluorophores on the gold nanoparticle from within the intracellular environment. The location of the nanosensor **3** within the CHO cells was established by co-localization with LysoSensor Green DND-189, a selective probe for acidic organelles. Importantly, by measuring the full spectrum of the two ligands on the pH nanosensor within the CHO cells a robust determination of localized pH from acidic organelles has been achieved.

The anthracene derivative ligand **1** was designed as a PET-based fluorescent pH reporter molecule, while the rhodamine derivative ligand **2** was designed as the ratiometric pair. Both ligands contained a thiol moiety as the terminal group ensuring that the organic ligands **1** and **2** spontaneously self-assembled to the surface of gold nanoparticles. Metallic particles, especially those based on gold, may quench fluorophores attached to the metal surface.[22] To prevent such excited state quenching, both ligands **1** and **2** were synthesized with a long alkyl chain that separated the thiol group from the anthracene and the rhodamine macrocycle respectively. The synthesis of the anthracene derivative ligand **1** was accomplished in three steps starting from 9-(chloromethyl)anthracene (see Scheme S1 in the Supporting Information). Ligand **1** emits fluorescence at 400–500 nm (λ_{exc} = 370 nm) in an acidic solution, when the tertiary amine is protonated. Following the classic PET mechanism,[20b] the fluorescence of ligand **1** is quenched in a neutral or alkaline medium (Figure S1). Ligand **2** was prepared by reaction of 5-(and-6)-carboxytetramethylrhodamine succinimidyl ester with 11-amino-undecanethiol (see Scheme S2 in the Supporting Information). The fluorescence emission intensity of **2** also varies as a function of pH with the intensity decreasing with increasing acidity (Figure S2). Ligand **2** emits fluorescence at 550–650 nm (λ_{exc} = 364 nm). Since ligands **1** and **2** emit in different regions of the visible spectrum they are ideal for ratiometric measurements.

Reduction of $HAuCl_4$ by $NaBH_4$ in DMF:H_2O solution (DMF = dimethylformamide) in the presence of equimolar amounts of **1** and **2**, yielded the stabilized ratiometric pH nanosensor **3** (Figure 1) which was characterized by transmission electron microscopy (TEM), UV/Vis spectroscopy and steady-state/time-resolved fluorimetry. TEM analysis revealed nonaggregated nanoparticles of (3.6 ± 0.9) nm average diameter (Figure S3). The UV/Vis spectrum of the dark purple solution of the pH nanosensor **3** exhibited an absorption band at 525–600 nm due to the rhodamine chromophore and an absorption band with the characteristic vibrational structure of the anthracenic moiety at 350–400 nm. The spectrum was dominated by the broad absorption, from 350 to 800 nm, due to the surface plasmon band of the gold core (Figure 2a).

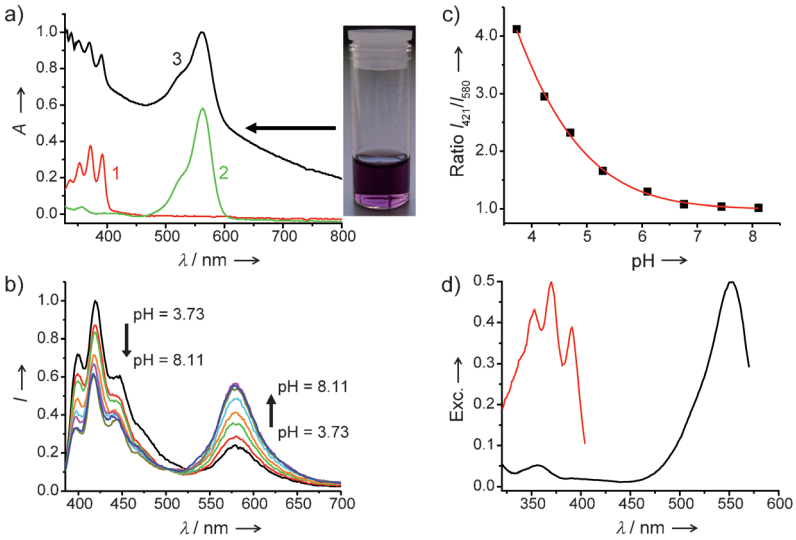

Figure 2. a) UV/Vis absorption spectra of **1**, **2**, and **3** in dimethyl sulfoxide (DMSO). Inset: A solution of the pH nanosensor **3**. b) Normalized fluorescence titration of nanosensor **3** as a function of pH in aqueous solution (11% DMSO) (λ_{exc} = 364 nm). c) pH titration curve of the pH nanosensor **3** using the fluorescence emission intensity ratio I_{421}/I_{580} as a function of pH (λ_{exc} = 364 nm). d) Fluorescence excitation (Exc.) spectra of nanosensor **3** (DMF:H_2O = 1:1) monitoring the emission at 450 (red) and at 580 nm (black).

Upon excitation at 364 nm of a solution of the pH nanosensor **3**, fluorescence emission of the two fluorophores was observed (Figure 2b). The spectrum showed an intense fluorescence emission with vibrational structure between 400 and 450 nm, from the anthracene ligand **1**, and a weaker emission band centered at 550–650 nm, from the rhodamine derivative **2**. The changing fluorescence emission spectrum of the nanosensor **3** with varying pH is shown in Figure 2b. It is apparent that a reduction of the fluorescence intensity of the anthracene emission concomitant with a similar increase of the fluorescence intensity due to the rhodamine ligand is observed when the pH of the medium is increased from 3.73 to 8.11. The ratio of fluorescence intensities from the two fluorophores (I_{421}/I_{580}) is therefore ideal for the estimation of pH (Figure 2c).

Since a single wavelength of 364 nm was used for the fluorescence excitation, interchromophoric interactions of the excited states could occur, leading to a free resonance energy transfer (FRET) process from anthracene to rhodamine.[23] To determine whether such an energy transfer process occurred, fluorescence excitation spectra of a solution of nanosensor **3** monitoring the emission of both fluorophores at 450 and 580 nm were recorded. As can be seen in Figure 2d, the fluorescence excitation profiles for both measurements correspond to separate species and hence suggests that the fluorescence emission of each chromophore on the nanoparticle is fully independent. Time-resolved measurements of the fluorescence of the ratiometric pH nanosensor **3** show that the primary lifetime of ligand **1** decreases on the gold surface (9.9 ns to 8.2 ns) while the

lifetime of ligand **2** remains almost constant (2.6 to 2.4 ns, Figure S4 and Table S1). The fluorescence quantum yield (ϕ) of ligands **1** and **2** and the two ligands on the pH nanosensor **3** have been measured (Table S2) and show that the fluorescence emission of both ligands on the gold nanoparticle remains measurable. The properties of each ligand attached to the surface of the gold nanoparticle appear to be those of the free ligands **1** and **2** measured in solution. The retention of the ligand characteristics following self-assembly onto the gold surface is a remarkable feature of the nanosensor **3** here presented.

Following the photophysical characterization of the pH nanosensor **3** and the demonstration of ratiometric measurements across acidic pH values, the potential for fluorescence imaging within the intracellular environment of living cells was determined. CHO cells were incubated with a solution of the nanosensor **3** for 3 h. Confocal fluorescence imaging of the CHO cells loaded with nanosensor **3** was achieved by exciting at 364 nm and collecting the fluorescence emission in two separate channels, namely, the blue channel (385–430 nm) and the red channel (560–615 nm). The fluorescence images in Figure 3a and 3b show the separate fluorescence

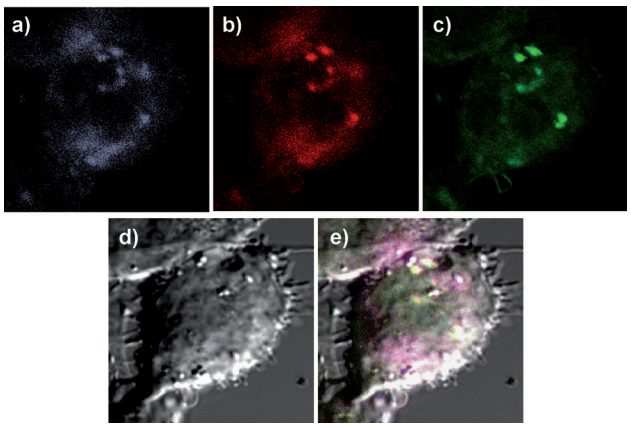

Figure 3. Confocal fluorescence microscopy images of a CHO cell incubated with the pH nanosensor **3** and DND-189. Fluorescence images collected in: a) blue channel (385–430 nm, $\lambda_{exc} = 364$ nm), b) red channel (560–615 nm, $\lambda_{exc} = 364$ nm), and c) green channel (505–530 nm, $\lambda_{exc} = 488$ nm). d) Differential interference contrast (DIC) image and e) composite images of blue, red, green, and DIC channels.

emission of the anthracene- and rhodamine-based fluorophores on the gold nanoparticle, respectively. The images from the blue and red channels coincide and such a spatial matching indicates that both ligands are attached to the gold nanoparticle surface within the cell. To elucidate the nature of the bright spots highlighted by the ratiometric pH nanosensor **3** (Figure 3a and 3b), LysoSensor DND-189, a selective probe for acidic organelles, was co-incubated with the nanoparticles. Figure 3c (green channel for 505–530 nm, $\lambda_{exc} = 488$ nm) highlights the fluorescence emission from DND-189. The co-localization of the pH nanosensor **3** with DND-189 is clearly demonstrated. Differential interference contrast (DIC) images of the CHO cells (Figure 3d) were collected simultaneously with the fluorescence images. When the images obtained from the DIC, blue, red, and green channels were overlaid, yellow spots were clearly visible (Figure 3e) which further highlight that the pH nanosensor **3** is co-located with the LysoSensor DND-189 in the acidic organelles. This result is in agreement with studies performed using electron microscopy that demonstrated that colloidal gold internalizes within cells following the endosomal–lysosomal pathway to finally accumulate in the lysosomes.[24]

While the high-quality images recorded using confocal fluorescence microscopy highlight the location of the pH nanosensor **3**, they are insufficient to conclusively assign the bright spots seen within the cell to the different fluorophores. However, the confocal microscope allows mapping of the complete fluorescence spectrum of whole cells from 367 to 688 nm and hence spectral (intensity versus wavelength) profiles can be determined. The confirmation that the anthracene (**1**) and rhodamine (**2**) based ligands were together inside the cell was achieved by recording the fluorescence emission spectrum of the cells loaded with the pH nanosensor **3** (Figure S5). In all of the 16 cell samples analyzed, it was possible to identify clearly the fluorescence emission resulting from the anthracene- and the rhodamine-based derivatives. Control experiments highlight the clear difference in the fluorescence emission spectrum obtained for the cells loaded with the pH nanosensor **3** and background fluorescence from the control cells (Figure S5).

Crucially, measurements of the pH values from within the acidic organelles of CHO cells have been obtained. Following the recording of the complete fluorescence emission of a CHO cell incubated with the pH nanosensor **3**, areas of interest within the cell were selected in order to obtain spectral profiles of specific zones. The series of 16 isolated cells were mapped and areas containing the pH nanosensor **3** were carefully analyzed. An illustrative example of this methodology for a selected cell is shown in Figure 4.

In Figure 4a two specific zones have been highlighted (A and B). The fluorescence emission spectra of these two zones (Figure 4b) show clear differences of the relative intensity of the anthracene- and the rhodamine-based ligands on the pH nanosensor **3**. A calibration curve of the fluorescence intensity ratio (I_{399}/I_{570}) versus pH, of a buffered solution, was obtained using the confocal microscope (Figure 4c) for the pH interval 3.47 to 6.52. Fluorescence emission intensities at 399 and 570 nm were selected since these were the intensity maxima corresponding to the anthracene and rhodamine ligands, respectively, obtained from the solution of nanosensor **3** using the confocal microscope (see Figure S6). From this calibration curve it was possible to estimate a pH value of 4.4 ± 0.2 for area A and a pH of 5.4 ± 0.3 for area B in the cell shown in Figure 4a. These are the expected values for lysosomes, which are reported to have a pH between 4.0 and 5.5. It is important to note that the calibration curve was obtained using the confocal microscope on the same day that the intracellular experiments were performed. The methodology here presented resulted in robust data since for all the pH estimations performed (83 regions in the 16 different cells studied in two different experiments) the mean pH value found was 5.2 ± 0.7, a value in agreement with the pH expected for acidic organelles. Furthermore, the pH reported

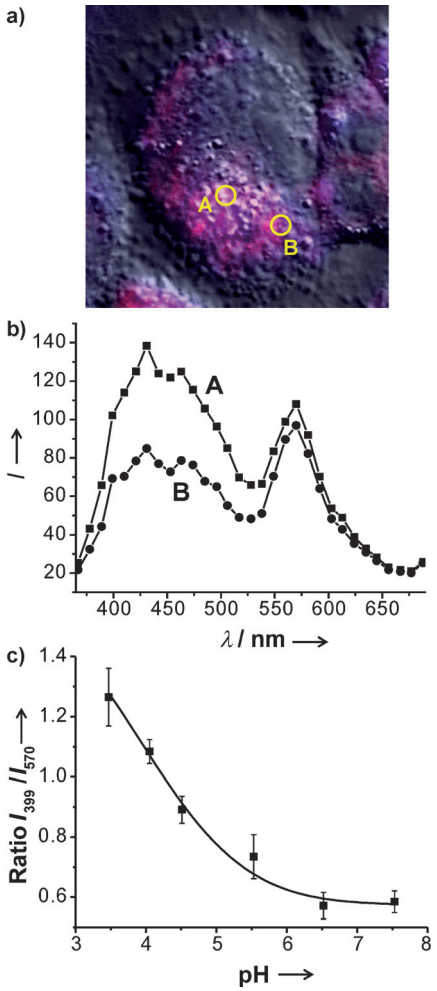

Figure 4. Estimation of intracellular pH. a) Confocal fluorescence microscopy image of a CHO cell incubated with the pH nanosensor **3** (λ_{exc} = 364 nm). b) Fluorescence emission spectra of areas A and B in image (a). c) pH titration curve of the pH nanosensor **3** obtained from the fluorescence emission intensity ratio I_{399}/I_{570} as a function of pH (λ_{exc} = 364 nm). The error bars show the standard deviation of the measurements. [$y = 3.39702 - 0.81079x + 0.05807x^2$].

by the fluorescence emission spectrum obtained from the whole cell was 5.1 ± 0.5. This value indicates that the ratiometric pH nanosensor **3** had accumulated in the acidic organelles within the intracellular environment.

In summary, we have reported the synthesis and characterization of a new dual emissive probe based on the self-assembly of two fluorescent ligands, that includes a PET-based pH sensor, to the surface of gold nanoparticles. The properties of the free ligands are transferred to the nano-assembly, that is, the fluorescence is not appreciably quenched by the gold nanoparticle and the pH sensitivity is maintained, leading to a ratiometric pH nanosensor for the estimation of acidity. The morphology and the internal compartmentalization of the cells are both retained suggesting that the ratiometric pH nanosensor **3** does not compromise cellular activity. The presence of the ratiometric pH nanosensor **3** inside the cell has been confirmed, for the first time, by the fluorescence emission spectrum from within the cell. Importantly, the pH of acidic organelles such as lysosomes has been determined using fluorescence ratiometric intracellular measurements. The results presented open the way for future developments of similar doubly self-assembled nanoprobes, not only targeting protons, but also a variety of analytes of biological interest.

Received: May 18, 2012
Published online: August 21, 2012

Keywords: photoinduced electron transfer · fluorescence · nanosensors · intracellular analysis · pH sensing

[1] a) J. R. Casey, S. Grinstein, J. Orlowski, *Nat. Rev. Mol. Cell Biol.* **2010**, *11*, 50–61; b) A. Haas, *Traffic* **2007**, *8*, 311–330; c) P. Paroutis, N. Touret, S. Grinstein, *Physiology* **2004**, *19*, 207–215.
[2] a) O. Warburg, *Science* **1956**, *123*, 309–314; b) S. M. Simon, M. Schindler, *Proc. Natl. Acad. Sci. USA* **1994**, *91*, 3497–3504; c) H. Izumi, T. Torigoe, H. Ishiguchi, H. Uramoto, Y. Yoshida, M. Tanabe, T. Ise, T. Murakami, T. Yoshida, M. Nomoto, K. Kohno, *Cancer Treat. Rev.* **2003**, *29*, 541–549.
[3] N. Piwon, W. Gunther, M. Schwake, M. R. Bosl, T. J. Jentsch, *Nature* **2000**, *408*, 369–373.
[4] M. Schindler, S. Grabski, E. Hoff, S. M. Simon, *Biochemistry* **1996**, *35*, 2811–2817.
[5] a) A. H. Futerman, G. van Meer, *Nat. Rev. Mol. Cell. Biol.* **2004**, *5*, 554–565; b) R. O. Brady, *Annu. Rev. Med.* **2006**, *57*, 283–296; c) E. Beutler, *Mol. Genet. Metab.* **2006**, *88*, 208–215; d) M. L. Schultz, L. Tecedor, M. Chang, B. L. Davidson, *Trends Neurosci.* **2011**, *34*, 401–410.
[6] J. Han, K. Burgess, *Chem. Rev.* **2010**, *110*, 2709–2728.
[7] a) T. Doussineau, A. Schulz, A. Lapresta-Fernandez, A. Moro, S. Korsten, S. Trupp, G. J. Mohr, *Chem. Eur. J.* **2010**, *16*, 10290–10299; b) Y. E. K. Lee, R. Smith, R. Kopelman, *Annu. Rev. Anal. Chem.* **2009**, *2*, 57–76; c) S. M. Buck, H. Xu, M. Brasuel, M. A. Philbert, R. Kopelman, *Talanta* **2004**, *63*, 41–59.
[8] a) H. A. Clark, M. Hoyer, M. A. Philbert, R. Kopelman, *Anal. Chem.* **1999**, *71*, 4831–4836; b) H. A. Clark, R. Kopelman, R. Tjalkens, M. A. Philbert, *Anal. Chem.* **1999**, *71*, 4837–4843.
[9] a) E. Pringsheim, D. Zimin, O. S. Wolfbeis, *Adv. Mater.* **2001**, *13*, 819–822; b) S. Horning, A. Schulz, G. J. Mohr, T. Heinze, *J. Photopolym. Sci. Technol.* **2009**, *22*, 671–673; c) G. R. Sun, H. G. Cui, L. Y. Lin, N. S. Lee, C. Yang, W. L. Neumann, J. N. Freskos, J. J. Shieh, R. B. Dorshow, K. L. Wooley, *J. Am. Chem. Soc.* **2011**, *133*, 8534–8543; d) H. H. Sun, K. Almdal, T. L. Andresen, *Chem. Commun.* **2011**, *47*, 5268–5270; e) V. M. Chauhan, G. R. Burnett, J. W. Aylott, *Analyst* **2011**, *136*, 1799–1801; f) S. Schreml, R. J. Meier, O. S. Wolfbeis, M. Landthaler, R. M. Szeimies, P. Babilas, *Proc. Natl. Acad. Sci. USA* **2011**, *108*, 2432–2437.
[10] a) S. Kim, H. E. Pudavar, P. N. Prasad, *Chem. Commun.* **2006**, 2071–2073; b) F. Gao, L. J. Tang, L. Dai, L. Wang, *Spectrochim. Acta Part A* **2007**, *67*, 517–521; c) T. Doussineau, S. Trupp, G. J. Mohr, *J. Colloid Interface Sci.* **2009**, *339*, 266–270; d) J. Y. Lei, L. Z. Wang, J. L. Zhang, *Chem. Commun.* **2010**, *46*, 8445–8447.
[11] a) P. T. Snee, R. C. Somers, G. Nair, J. P. Zimmer, M. G. Bawendi, D. G. Nocera, *J. Am. Chem. Soc.* **2006**, *128*, 13320–13321; b) J. D. Krooswyk, C. M. Tyrakowski, P. T. Snee, *J. Phys. Chem. C* **2010**, *114*, 21348–21352; c) T. Jin, A. Sasaki, M. Kinjo, J. Miyazaki, *Chem. Commun.* **2010**, *46*, 2408–2410; d) K. Paek, S. Chung, C.-H. Cho, B. J. Kim, *Chem. Commun.* **2011**, *47*, 10272–10274.
[12] L. J. Nielsen, S. Eyley, W. Thielemans, J. W. Aylott, *Chem. Commun.* **2010**, *46*, 8929–8931.

[13] T. Myochin, K. Kiyose, K. Hanaoka, H. Kojima, T. Terai, T. Nagano, *J. Am. Chem. Soc.* **2011**, *133*, 3401 – 3409.
[14] T. Doussineau, M. Smaihi, G. J. Mohr, *Adv. Funct. Mater.* **2009**, *19*, 117 – 122.
[15] a) S. Hornig, C. Biskup, A. Grafe, J. Wotschadlo, T. Liebert, G. J. Mohr, T. Heinze, *Soft Matter* **2008**, *4*, 1169 – 1172; b) H. H. Sun, T. L. Andresen, R. V. Benjaminsen, K. Almdal, *J. Biomed. Nanotechnol.* **2009**, *5*, 676 – 682; c) A. Schulz, J. Wotschadlo, T. Heinze, G. J. Mohr, *J. Mater. Chem.* **2010**, *20*, 1475 – 1482; d) X. J. Wang, C. Boschetti, M. J. Ruedas-Rama, A. Tunnacliffe, E. A. H. Hall, *Analyst* **2010**, *135*, 1585 – 1591.
[16] a) S. E. Stanca, S. Nietzsche, W. Fritzsche, C. G. Cranfield, C. Biskup, *Nanotechnology* **2010**, *21*; b) H. S. Peng, J. A. Stolwijk, L. N. Sun, J. Wegener, O. S. Wolfbeis, *Angew. Chem.* **2010**, *122*, 4342 – 4345; *Angew. Chem. Int. Ed.* **2010**, *49*, 4246 – 4249.
[17] a) Y. L. Chiu, S. A. Chen, J. H. Chen, K. J. Chen, H. L. Chen, H. W. Sung, *ACS Nano* **2010**, *4*, 7467 – 7474; b) S. Wu, Z. Li, J. Han, S. Han, *Chem. Commun.* **2011**, *47*, 11276 – 11278.
[18] a) A. Burns, P. Sengupta, T. Zedayko, B. Baird, U. Wiesner, *Small* **2006**, *2*, 723 – 726; b) J. Peng, X. He, K. Wang, W. Tan, Y. Wang, Y. Liu, *Anal. Bioanal. Chem.* **2007**, *388*, 645 – 654; c) Y. H. Chan, C. F. Wu, F. M. Ye, Y. H. Jin, P. B. Smith, D. T. Chiu, *Anal. Chem.* **2011**, *83*, 1448 – 1455; d) Y.-P. Chen, H.-A. Chen, Y. Hung, F.-C. Chien, P. Chen, C.-Y. Mou, *RSC Adv.* **2012**, *2*, 968 – 973.
[19] R. V. Benjaminsen, H. Sun, J. R. Henriksen, N. M. Christensen, K. Almdal, T. L. Andresen, *ACS Nano* **2011**, *5*, 5864 – 5873.
[20] a) A. P. de Silva, H. Q. Gunaratne, T. Gunnlaugsson, A. J. Huxley, C. P. McCoy, J. T. Rademacher, T. E. Rice, *Chem. Rev.* **1997**, *97*, 1515 – 1566; b) A. P. de Silva, T. S. Moody, G. D. Wright, *Analyst* **2009**, *134*, 2385 – 2393; c) M. I. Burguete, F. Galindo, M. A. Izquierdo, S. V. Luis, L. Vigara, *Tetrahedron* **2007**, *63*, 9493 – 9501.
[21] F. Galindo, M. I. Burguete, L. Vigara, S. V. Luis, N. Kabir, J. Gavrilovic, D. A. Russell, *Angew. Chem.* **2005**, *117*, 6662 – 6666; *Angew. Chem. Int. Ed.* **2005**, *44*, 6504 – 6508.
[22] a) G. Schneider, G. Decher, N. Nerambourg, R. Praho, M. H. Werts, M. Blanchard-Desce, *Nano Lett.* **2006**, *6*, 530 – 536; b) S. Y. Lim, J. H. Kim, J. S. Lee, C. B. Park, *Langmuir* **2009**, *25*, 13302 – 13305; c) A. Kotiaho, R. Lahtinen, A. Efimov, H. K. Metsberg, E. Sariola, H. Lehtivuori, N. V. Tkachenko, H. Lemmetyinen, *J. Phys. Chem. C* **2010**, *114*, 162 – 168.
[23] J. R. Lakowicz, *Principles of fluorescence spectroscopy*, 2nd ed., Kluwer Academic/Plenum, New York, **1999**.
[24] a) L. Hosta, M. Pla-Roca, J. Arbiol, C. Lopez-Iglesias, J. Samitier, L. J. Cruz, M. J. Kogan, F. Albericio, *Bioconjugate Chem.* **2009**, *20*, 138 – 146; b) F. Porta, Z. Krpetic, L. Prati, A. Gaiassi, G. Scari, *Langmuir* **2008**, *24*, 7061 – 7064; c) H. Yang, S.-Y. Fung, M. Liu, *Angew. Chem.* **2011**, *123*, 9817 – 9820; *Angew. Chem. Int. Ed.* **2011**, *50*, 9643 – 9646.

